Heterogeneous metasomatism in cumulate xenoliths from the Spanish Central System: implications for percolative fractional crystallization of lamprophyric melts

D. OREJANA & C. VILLASECA

Department of Petrology and Geochemistry, Complutense University of Madrid, Madrid 28040, Spain (e-mail: dorejana@geo.ucm.es)

Abstract: The alkaline lamprophyres and diabases from the Spanish Central System carry a heterogeneous suite of xenoliths including a group of highly altered ultramafic pyroxenites that contain Cr–Mg-rich high-*T* hydrous minerals (Ti-phlogopite and pargasitic to kaersutitic amphibole), indicative of modal metasomatism. The trace element mineral compositions of these xenoliths show three patterns: type A xenoliths, with light rare earth element enriched clinopyroxenes with high field strength element (HFSE) negative anomalies; type B xenoliths, with clinopyroxenes and amphiboles with high incompatible trace element contents (large ion lithophile elements (LILE), HFSE and REE); type C xenoliths, with relatively REE- and HFSE-poor clinopyroxenes and amphiboles. These metasomatic signatures suggest the involvement of three different metasomatic agents: carbonate, silicate and hydrous fluids or melts, respectively. These agents could have been derived from the progressive differentiation of a CO_2–H_2O-rich highly alkaline magma, genetically related to the Late Permian alkaline magmatism. Because of the original sub-alkaline nature of the pyroxenite xenoliths, they might have been formed originally as pyroxene-rich cumulates associated with underplated Hercynian calc-alkaline basic magmas. Metasomatism as a result of the infiltration of alkaline magmas within these cumulates might explain the relatively high radiogenic Nd composition of the altered ultramafic xenoliths.

Ultramafic xenoliths carried by mantle-derived alkaline volcanic and subvolcanic magmas sometimes include pyroxenitic types, which are much less abundant than typical mantle lithologies (peridotites). Several possible origins have been proposed for pyroxenite xenoliths: (1) cumulates or segregations from mantle-derived magmas introduced as dykes or veins within the lithospheric mantle (e.g. Frey & Prinz 1978; Downes 2001); (2) cumulates crystallized within deep magma chambers near the upper mantle–lower crust boundary, associated with underplating of mafic magmas (e.g. Fémenias *et al.* 2003); (3) restites produced during melting and genetically associated with overlying orogenic batholiths (Ducea & Saleeby 1998); (4) remnants of oceanic crust, subducted into the asthenosphere and then streaked out by mantle convection until they were incorporated into the lithosphere (Allègre & Turcotte 1986). Moreover, some pyroxenites have been subjected to a later enrichment process (Garrido & Bodinier 1999; Litasov *et al.* 2000; Xu 2002).

The Upper Permian alkaline lamprophyres and diabases from the Spanish Central System (SCS) carry a heterogeneous xenolith suite, including lower crustal granulites (Villaseca *et al.* 1999) and ultramafic pyroxenites and hornblendites (Orejana *et al.* 2006). Some types of pyroxenites have never been studied because of their scarcity and alteration. These altered pyroxenites show a relict high-*T* paragenesis composed of clinopyroxene, amphibole and phlogopite, pointing to the involvement of a metasomatic transformation at depth.

The nature of the metasomatizing agents in enrichment processes can be broadly divided into three categories: (1) silicate melts (e.g. Ionov *et al.* 2002*a*; Witt-Eickschen *et al.* 2003); (2) carbonate or carbonatitic melts and/or fluids (e.g. Ionov 1998; Yaxley *et al.* 1998; Xu *et al.* 2003); (3) hydrous fluids (e.g. Johnson *et al.* 1996).

The presence of multiple types of geochemical patterns in a single suite of ultramafic xenoliths is relatively common and sometimes has led to the conclusion that various genetically unrelated liquids were involved (Grégoire *et al.* 2003; Witt-Eickschen *et al.* 2003), whereas, in other cases, it has been interpreted as being derived from different metasomatic agents genetically related to a single original melt by percolative fractional crystallization (Litasov *et al.* 2000; Ionov *et al.* 2002*a*; Xu & Bodinier 2004). The widely accepted porous melt flow model (Navon & Stolper 1987) predicts the possibility of generation of volatile-rich (H_2O–CO_2) melts or fluids from a single volatile-rich magma (Downes 2001; Xu & Bodinier 2004) as a result of a continuous reaction with the rock matrix. These low-viscosity agents

are capable of producing a strong interaction with the wall rock.

This paper focuses on the petrography and the major and trace element mineral composition of the altered pyroxenite SCS xenoliths, with the intention of constraining their origin, and discusses the interaction with metasomatic agents and their relationship with the host alkaline basic magmas at different emplacement levels.

Geological background

The SCS is a plutonic–metamorphic terrane composed of several Hercynian granitic intrusions, emplaced into Neoproterozoic metasediments and Palaeozoic orthogneisses (Fig. 1). This basement is crosscut by several post-orogenic dyke swarms with contrasting geochemical affinities: calc-alkaline, shoshonitic, alkaline and tholeiitic (Villaseca *et al.* 2004). The alkaline suite can be divided in two groups: (1) basic to ultrabasic lamprophyres (camptonites) and diabases; (2) red monzo-syenitic porphyries. Geochronological data on this alkaline magmatism yield an age of intrusion in the range 252–264 Ma (264 Ma, Ar–Ar in amphibole, Perini *et al.* 2004; Scarrow *et al.* 2006; or 252 Ma, U–Pb in zircon, Fernández-Suárez *et al.* 2006).

The SCS alkaline magmatism occurred in an anorogenic setting during the initial stages of North Atlantic opening. Orogenic Hercynian metamorphism in the area reached its peak at around 330 Ma and afterwards experienced a marked retrograde cooling path associated with moderate uplift (Escuder Viruete *et al.* 1998). During these post-orogenic conditions, voluminous granitic and calc-alkaline magmas intruded these crustal levels, promoting important local contact metamorphism. At 70 Ma after the regional metamorphism, during Late Permian times, lamprophyre dyke swarms were emplaced at very shallow and cool levels, although this did not result in contact metamorphism because of the small volume of magma. These uplifted crustal blocks into which the lamprophyres were intruded have not experienced burial since Early Mesozoic times, as revealed by fission-track data (Bruijne & Andriessen 2000). Moreover, a significant hydrothermal imprint is not observed in either the lamprophyre dykes or the plutono-metamorphic wall rocks, suggesting long-term stable crustal conditions after the alkaline magmatism. Therefore, the significant degree of alteration shown by the studied pyroxenite xenoliths suggests a genetic relationship with the host lamprophyric melt as discussed below.

The SCS alkaline lamprophyres and diabases carry a wide variety of xenolithic material, comprising wall-rock fragments (granites and gneises), lower crustal xenoliths (granulites *sensu lato*) and mafic to ultramafic pyroxene-rich cumulates from the upper mantle–lower crust boundary. This last group of xenoliths has been divided, in previous studies, in four subgroups according to their petrographic characteristics (Orejana *et al.* 2006): (1) highly altered xenoliths; (2) spinel pyroxenites; (3) hydrated clinopyroxenites; (4) magmatic amphibole-rich clinopyroxenites and hornblendites.

Type 2 spinel pyroxenites and type 4 hornblendites are generally larger in size and more abundant than the other ultramafic xenoliths (Orejana *et al.* 2006). They have been interpreted as magmatic cumulates or segregates crystallized at the upper mantle–lower crust boundary. The amphibole-rich type 4 xenoliths show magmatic textures, and have been interpreted as crystallizing from the alkaline melts (Orejana *et al.* 2006). In contrast, type 2 xenoliths display a granoblastic texture and, occasionally, also contain orthopyroxene (e.g. websterite 102131). Thus, they have been interpreted as being related to earlier magmatic events associated with underplating of calc-alkaline basic magmas at the base of the crust (Orejana *et al.* 2006).

Types 1 and 3 ultramafic xenoliths of Orejana *et al.* (2006) show a variable amount of high-*T* hydrated phases (amphibole and phlogopite). Nevertheless, their crystalloblastic fabric and modal mineral composition differentiate them from the clearly igneous-textured type 4 xenoliths (also rich in amphibole or phlogopite). Their scarcity and small size represent major hindrances to their study, especially when considering their whole-rock and isotope geochemistry.

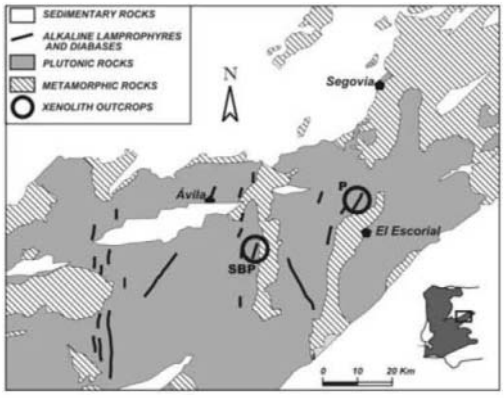

Fig. 1. Sketch map of the Spanish Central System showing the location of the Permian alkaline lamprophyres and diabases, and the outcrops of the altered ultramafic xenoliths (P, Peguerinos; SBP, San Bartolomé de Pinares).

Nevertheless, in this paper we present a general petrographic and geochemical characterization of these enclaves, mainly focusing on major and trace element mineral composition, although whole-rock geochemical analyses and Sr–Nd isotope determinations have been carried out on two samples.

Analytical methods

The major element mineral composition has been analysed at the Centro de Microscopía Electrónica 'Luis Bru' (Complutense University of Madrid) using a Jeol JZA-8900 M electron microprobe with four wavelength-dispersive spectrometers. Analytical conditions were an accelerating voltage of 15 kV and an electron beam current of 20 nA, with a beam diameter of 5 μm. Elements were counted for 10 s on the peak and 5 s on each background position. Corrections were made using the ZAF method.

We have determined *in situ* the concentrations of 27 trace elements (rare earth elements (REE), Ba, Rb, Th, U, Nb, Ta, Pb, Sr, Zr, Hf, Y, V, Cr and Ni) in clinopyroxene, amphibole and phlogopite, on >130 μm thick polished sections by laser ablation inductively coupled plasma mass spectrometry (LA-ICP-MS) at the University of Bristol using a VG Elemental PlasmaQuad 3 ICP-MS system coupled to a VG LaserProbe II (266 nm frequency-quadrupled Nd–YAG laser). The counting time for one analysis was typically 100 s (40 s measuring gas blank to establish the background and 60 s for the remainder of the analysis). The diameter of laser beam was around 20 μm. The NIST 610 and 612 glass standards were used to calibrate relative element sensitivities for the analyses of the silicate minerals. Each analysis was normalized to Ca using concentrations determined by electron microprobe.

The whole-rock major and trace element composition of two xenoliths was analysed at the CNRS-CRPG Nancy. The samples were melted using $LiBO_2$ and dissolved with HNO_3. Solutions were analysed by inductively coupled plasma atomic emission spectrometry (ICP-AES) for major elements, whereas trace elements were determined by ICP-MS. Uncertainties in major elements are bracketed between 1 and 3%, except for MnO (5–10%) and P_2O_5 (>10%). Carignan *et al.* (2001) have evaluated the precision of Nancy ICP-MS analyses at low concentration levels from repeated analyses of the international standards BR, DR-N, UB-N, AN-G and GH. The precision for Rb, Sr, Zr, Y, V, Hf and most of the REE are in the range 1–5%, whereas they range from 5 to 10% for the other trace elements, including Tm. More information on the procedure, precision and accuracy of Nancy ICP-MS analyses has been given by Carignan *et al.* (2001).

Sr–Nd isotopic analyses of two xenoliths were carried out at the CAI de Geocronología y Geoquímica Isotópica of the Complutense University of Madrid, using an automated VG Sector 54 multicollector thermal ionization mass spectrometer with data acquired in multidynamic mode. Isotopic ratios of Sr and Nd were measured on a subset of whole-rock powders. The analytical procedures used in this laboratory have been described elsewhere (Reyes *et al.* 1997). Repeated analysis of NBS 987 gave $^{87}Sr/^{86}Sr = 0.710249 \pm 30$ (2σ, $n = 15$) and for the JM Nd standard $^{143}Nd/^{144}Nd = 0.511809 \pm 20$ (2σ, $n = 13$). The 2σ error on ε(Nd) calculation is ± 0.4. An estimated age of 265 Ma was used for calculating initial isotopic ratios.

Petrography of xenoliths

Although the altered pyroxenite xenolith suite has been previously classified into two types, the similarity of their petrography (high degree of alteration and the common presence of high-temperature hydrated minerals), suggests that they all form a heterogeneous, genetically related group. Thus, for the sake of simplicity, we shall refer to them hereafter as altered ultramafic SCS xenoliths.

These altered ultramafic SCS xenoliths have been sampled at two outcrops: Peguerinos (P) and San Bartolomé de Pinares (SBP) (Fig. 1). They are small in size, never exceeding 2.7 cm, and are irregular to semi-rounded in shape. Their modal composition is summarized in Table 1.

SCS altered pyroxenite xenoliths are composed of variable amounts of two mineral parageneses: (1) a granoblastic high-*T* assemblage of clinopyroxene, amphibole, phlogopite and spinel; (2) a later, volatile-rich alteration assemblage of chlorite group and talc minerals that pseudomorph granoblastic crystals. The texture of the altered ultramafic SCS xenoliths is fine-grained, equigranular and granoblastic, showing typical triple junctions indicative of solid-state equilibration. This high-*T* crystalloblastic fabric is preserved irrespective of the degree of secondary alteration.

Mineral heterogeneity might be related to the small size of these xenoliths, giving rise to a wide range of modal composition. Moreover, the lack of olivine suggests a cumulate origin instead of representing mantle fragments. Primary high-*T* minerals are restricted to uncoloured clinopyroxene, pargasitic to kaersutitic amphibole, Ti-phlogopite and brown spinel (Table 1). Clinopyroxene modal

Table 1. *Modal analyses of SCS altered xenoliths*

Sample:	104394	104546B	105776	105787	103656-1	103656-2	103657B-1	103657B-2	103657B-3	104534A	104535	104540A	105788
Locality:	P	P	P	SBP	SBP	SBP	SBP	SBP	SBP	SBP	SBP	SBP	SBP
Type:	A	B	A	C	B	B	B	B	B	B	B	B	B
Cpx	9.5	18.2	10.5	16.4	2.6	58.2	35.0	21.9	9.6	74.3	41.4	80.9	9.3
Amph		3.0		1.7	1.3		16.0			5.4	3		10.8
Phl					0.7		12.0						3.2
Sp	2.7	3.0	3.0	3.1					0.9		6.1		
Sulph.	1.8	3.0							89.5		49.5	19.1	76.7
Sec.min.	86.0	72.8	86.5	78.8	95.4	41.8	37.0	78.1		20.3			
Size (cm)	1.5 × 0.3	0.6 × 0.5	2.3 × 0.6	0.7 × 1	0.5 × 0.6	0.7 × 0.3	0.2 × 0.2	1.1 × 0.6	0.9 × 0.45	0.3 × 0.3	0.3 × 0.6	0.3 × 0.7	0.8 × 1.1

P, Peguerinos; SBP, San Bartolomé de Pinares. Sec.min., secondary minerals.

proportion ranges from 2.6 to 81%. Spinel, amphibole and phlogopite are not always all present in these xenoliths. Although spinel is regularly disseminated when it appears, amphibole and phlogopite are more dispersed. Neither mineral zoning nor pyroxene exsolution lamellae have been observed in these high-*T* minerals.

These pyroxenite xenoliths have secondary minerals in variable proportions from 19 to 95%. These alteration phases are mainly talc and chlorite group minerals, pale brownish chlorite being the most common. Unaltered orthopyroxene has never been observed in these xenoliths. Olivine pseudomorphs are unlikely because the presence of this mineral in the original paragenesis is very limited according to their normative composition as deduced from whole-rock chemistry: *Ol* does not exceed 9%, whereas *Hy* ranges from 80 to 99% (see Table 4). The normative compositions of analysed samples plot within the field of orthopyroxenite in the ultramafic rocks classification diagram, pointing to orthopyroxene as the main original mafic phase (now pseudomorphed) in the modal composition of these xenoliths. In summary, normative and modal compositions point to a wide range of altered pyroxenites probably including orthopyroxenites and websterites.

The mineral chemistry of chlorite pseudomorphs also supports the interpretation that orthopyroxene was the main primary mineral of these pyroxenite xenoliths. When comparing the chemical composition of the abundant chloritized pseudomorphs with secondary chlorite from the partial replacement of orthopyroxene from the websterite sample 102131 (type 2 xenoliths of Orejana *et al.* 2006) we notice the good overlap of the two compositional fields (Fig. 2). Furthermore, the pale brownish colour and the good cleavage of both chlorite crystals reinforce the suggestion that they belong to the same chlorite type. The wide chemical composition shown by these chlorites suggests complex chemical substitution processes towards talc end-member compositions (Fig. 2). Talc and occasional Fe-sulphide are other secondary mineral phases.

Mineral chemistry

According to mineral chemistry, we have classified the altered xenoliths into three sub-types by their trace element contents (mainly light rare earth elements (LREE) in clinopyroxene and amphibole): type A xenoliths, with Sr–LREE-enriched clinopyroxene and lacking high-*T* hydrous phases (amphibole or phlogopite); type B xenoliths, with LREE-enriched clinopyroxene and amphibole; and type C xenoliths, with REE-poor clinopyroxene and amphibole.

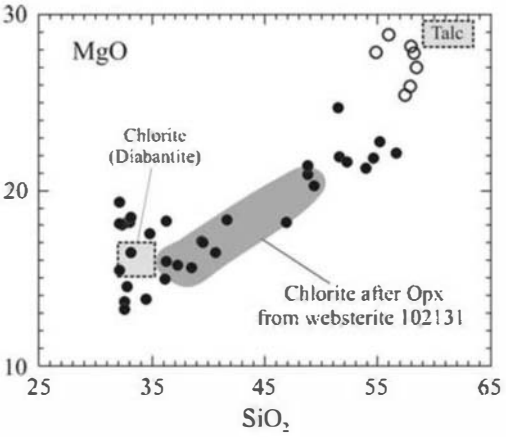

Fig. 2. Major element contents of secondary alteration minerals of the ultramafic SCS xenoliths (●, brownish chlorite ●, talc). Talc and chlorite (diabantite) compositional fields taken from data summarized by Deer *et al.* (1976).

Major elements

Clinopyroxene is diopside and augite with a heterogeneous major and trace element composition (Tables 2 and 3). Al_2O_3, TiO_2 and Na_2O may reach high concentrations: 4.2–7.7 wt%, 0.3–1.4 wt% and 0.41–1.75 wt%, respectively. Nevertheless, the heterogeneity shown by the major element composition highlights the large compositional ranges shown by clinopyroxenes from type B xenoliths (Fig. 3). This latter group has Mg-number values ranging from 0.78 to 0.93, whereas types A and C are restricted to Mg-number = 0.89–0.93 and are generally homogeneous with respect to major element composition, except for Na (Fig. 3).

Amphibole is absent in type A xenoliths (Table 1). Similar to what is observed for clinopyroxene, amphibole major and trace element composition is heterogeneous for type B xenoliths (Fig. 3). On the whole, they are Ti–Al-rich pargasites or kaersutites (TiO_2: 1.9–5.1 wt%; Al_2O_3: 12.9–15.7 wt%), with Na_2O in the range 2.2–3.3 wt%, K_2O from 0.71 to 1.84 wt% and high Mg-number (0.73–0.89), which overlaps the values for clinopyroxene (Table 2). Type C amphiboles do not differ significantly in their major element composition from type B (Fig. 3), but have higher Cr contents (7436–7845 ppm, compared with 2004–3236 ppm for type B; Table 3).

Phlogopite is present only in type B xenoliths (Table 1). Its major element composition is homogeneous, with Mg-number ranging from 0.82 to 0.86, overlapping the values for clinopyroxene and amphibole (Table 2). They typically have high TiO_2 (2.46–5.14 wt%), Cr_2O_3 (0.42–1.11 wt%) and Al_2O_3 (15.6–16.8 wt%) contents (Fig. 3). This composition contrasts with the lower Mg-number and Cr contents, and higher Ti concentrations of phlogopites from the SCS hornblenditic xenoliths, which have been interpreted as magmatic segregates genetically linked to the host alkaline melts (Grejana *et al.* 2006), and also with phlogopites from typical cumulate xenoliths (Fig. 3); but it is very similar to that of phlogopites from metasomatic ultramafic xenoliths, such as those reported by Shaw (2004). Because of the scarcity and small size of phlogopite from the altered ultramafic SCS xenoliths, we could not analyse their trace element composition.

Spinel is present in the three altered ultramafic SCS xenolith types. It is always Al–Cr-rich and Ti-poor, with Cr_2O_3 ranging from 4.8 to 14.3 wt%, Al_2O_3 from 49.7 to 63.5 wt%, TiO_2 < 0.22 wt% and Mg-number from 0.69 to 0.79 (Table 2). Nevertheless, spinel from type B xenoliths shows the lowest Cr_2O_3 and highest Al_2O_3 concentrations (4.8 and 63.5 wt%, respectively). Spinel of type A and C xenoliths displays the same narrow compositional range: 11.3–14.3 wt% for Cr_2O_3 and 49.7–55.9 wt% for Al_2O_3.

Trace elements

Clinopyroxene trace element characteristics emphasize the existence of three types of altered ultramafic xenoliths (Fig. 4a). Clinopyroxenes from type A xenoliths display the most LREE-enriched patterns, which may reach 100 times chondrite values, whereas heavy REE (HREE) tend to converge to concentrations shown by clinopyroxenes from the other two xenolith types. This LREE enrichment is also accompanied by high contents of Sr (208–230 ppm), but low values for Zr (22–26 ppm) and Nb (0.12–0.24 ppm) (Table 3). Accordingly, their primitive mantle-normalized trace element pattern is distinctive, with strong negative anomalies at Zr-Hf and Nb-Ta, and at Ba and Ti (Fig. 4b). Type B clinopyroxenes are also enriched in LREE, but with lower concentrations than type A. Moreover, they yield convex-upwards chondrite-normalized REE patterns with the peak position between Ce and Nd, which is characteristic of clinopyroxenes formed as deep cumulates crystallized from basic alkaline magmas (Irving & Frey 1984) (Fig. 4a). Nevertheless, the LREE concentrations of type B clinopyroxenes are significantly higher than those shown by Irving & Frey (1984). The primitive mantle-normalized trace element pattern of these clinopyroxenes is very similar to that of type A, but concentrations of Zr (32.1–72.5 ppm), Hf

Table 2. *Major element composition and P–T estimates of representative high-T minerals from the SCS altered ultramafic xenoliths*

Type:	Clinopyroxene A	Clinopyroxene B	Clinopyroxene B	Clinopyroxene B	Clinopyroxene C	Amphibole B	Amphibole B	Amphibole B	Amphibole C	Amphibole C	Phlogopite B	Phlogopite B	Phlogopite B	Spinel A	Spinel B	Spinel C
Sample:	104394 13	104546B 25	104534A 33	104535 26	105787 45	104546B 23	105788 33	104535 24	105787 46	105787 47	103656-1 36	103657B-1 4	105788 40	104394 5	104546B 22	105787 43
SiO_2	51.28	50.27	50.92	50.42	50.58	41.68	40.77	41.21	41.26	42.21	37.48	36.93	37.47	0.03	0.06	0.07
TiO_2	0.48	0.79	0.82	0.54	0.31	4.25	4.32	2.87	1.98	2.05	2.46	4.92	3.40	0.13	0.16	0.12
Al_2O_3	5.83	7.46	7.26	5.63	5.99	15.34	14.24	13.19	14.57	14.99	15.75	15.81	16.76	55.91	63.47	53.09
FeO^T	2.44	3.23	6.45	6.89	2.90	3.60	6.63	9.25	4.26	4.08	7.26	7.41	5.98	11.33	4.79	13.01
Cr_2O_3*	0.79	0.35	0.19	0.42	0.87	–	–	–	–	–	1.11	0.76	0.69	10.94	10.29	13.13
MnO	0.09	0.07	0.05	0.10	0.04	0.13	0.07	0.08	0.04	0.00	0.04	0.03	0.07	0.08	0.08	0.07
MgO	16.02	15.48	13.68	13.73	15.24	16.33	14.38	13.60	16.99	17.22	20.03	18.69	19.93	20.51	21.33	20.61
CaO	22.98	20.33	19.41	20.08	20.87	10.94	11.51	10.75	10.50	11.11	0.02	0.03	0.06	0.00	0.00	0.00
Na_2O	0.95	1.02	1.27	1.55	1.59	3.09	2.49	3.18	3.08	3.09	1.22	0.87	0.64	0.00	0.00	0.00
K_2O	0.00	0.00	0.00	0.00	0.00	1.04	1.71	0.74	1.12	1.05	8.84	9.08	9.15	0.00	0.00	0.01
Total	100.86	99.00	100.05	99.36	98.39	96.40	96.12	94.87	93.80	95.80	94.21	94.53	94.15	98.93	100.18	100.11
Mg-no.	0.92	0.89	0.83	0.78	0.90	0.89	0.79	0.72	0.88	0.88	0.83	0.82	0.86	0.77	0.79	0.74
Cations calculated on the basis of 6 O for clinopyroxene; 24 (O, OH, F) for amphibole; 24 (O, OH, F, Cl) for phlogopite; 32 O for spinel																
Si	1.837	1.835	1.837	1.856	1.853	6.854	7.491	6.395	6.196	6.062	5.720	5.620	5.680	0.010	0.010	0.010
Ti	0.013	0.022	0.039	0.015	0.008	0.526	0.597	0.335	0.224	0.221	0.280	0.560	0.390	0.020	0.020	0.020
Al	0.246	0.321	0.213	0.245	0.259	2.970	3.081	2.410	2.577	2.535	2.830	2.835	2.990	13.820	15.030	13.190
Fe	0.073	0.099	0.170	0.212	0.088	0.495	1.019	1.200	0.535	0.490	0.930	0.940	0.760	1.880	0.760	2.170
Cr	0.022	0.010	0.010	0.012	0.025	0.075	0.059	0.074	0.151	0.143	0.130	0.090	0.080	1.920	1.730	2.320
Mn	0.003	0.002	0.002	0.003	0.001	0.018	0.011	0.011	0.005	0.000	0.010	0.000	0.010	0.010	0.010	0.010
Mg	0.856	0.842	0.836	0.754	0.832	4.003	3.939	3.146	3.804	3.687	4.560	4.240	4.500	6.420	6.390	6.480
Ca	0.882	0.795	0.844	0.792	0.819	1.927	2.266	1.787	1.690	1.709	0.000	0.000	0.010	0.000	0.000	0.000
Na	0.066	0.072	0.048	0.111	0.113	0.985	0.887	0.957	0.897	0.861	0.360	0.260	0.190	0.000	0.000	0.000
K	0.000	0.000	0.001	0.000	0.000	0.218	0.401	0.146	0.215	0.192	1.720	1.760	1.770	0.000	0.000	0.000
ΣCations	3.998	3.998	4.000	4.000	3.998	18.071	19.751	16.461	16.294	15.900	16.540	16.305	16.380	24.080	23.950	24.200
T (°C)†	896	1049	1092	1078	988	1004	1009	966	937	938						
P (kbar)†	6.7	9.9	10.7	7.6	10.2											

*Cr contents in amphibole have been determined by LA-ICP-MS (see Table 3).

†*T* estimations calculated using single pyroxene and Al–Ti in amphibole thermometers of Mercier (1980) and Otten (1984), respectively. *P* estimations calculated using the barometer of Nimis & Ulmer (1998).

Table 3. *Trace element composition of representative clinopyroxenes and amphiboles from SCS altered ultramafic xenoliths*

	Clinopyroxene									Amphibole							
Type:	A	A	A	B	B	B	C	C	C	B	B	B	B	B	C	C	C
Sample:	104394	104394	104394	104546B	104535	104534A	105787	105787	105787	104546B	104546B	104534A	104534A	104534A	105787	105787	105787
	12	21	51	41	33	41	10	7	9	31	33	22	23	24	1	2	3
Ba	0.84	1.37	2.42	1.57	0.92	3.92	2.60	2.17	bd	172	178	236	247	228	79.7	82.1	84.3
Rb	bd	bd	1.65	bd	0.67	0.43	0.65	0.47	bd	4.84	5.12	6.01	6.03	6.20	5.69	5.97	6.33
Sr	230	212	215	95.3	107.6	101.2	44.8	44.0	40.9	278	208	474	488	504	120	120	117
Pb	na	na	na	na	na	na	0.46	0.16	0.17	na	na	na	na	na	0.29	0.45	0.43
Th	0.06	0.10	0.08	0.31	0.24	0.14	bd	bd	0.06	0.20	0.33	0.15	0.16	0.19	bd	bd	bd
U	bd	bd	0.03	0.09	0.08	0.05	bd	bd	bd	0.05	0.11	0.03	0.05	0.04	bd	bd	bd
Zr	24.5	24.8	25.9	38.4	70.5	56.2	17.5	16.7	16.4	66.7	73.2	52.6	51.8	52.6	16.8	18.0	15.6
Nb	0.10	0.17	0.13	1.56	0.27	0.59	0.16	bd	0.11	78.4	53.2	43.1	45.3	45.2	1.35	1.23	1.36
Y	16.8	15.5	14.9	19.9	24.4	18.6	16.7	15.5	15.1	21.7	21.8	21.7	22.7	21.8	17.3	18.2	17.8
V	254	246	251	286	623	709	344	320	319	440	450	909	944	905	501	545	543
Ni	393	404	386	315	116	74	432	286	325	605	596	129	149	129	na	na	na
Cr	5215	4948	5020	2046	2892	1745	5239	4687	5310	3124	3236	2087	2182	2118	7436	7845	7721
Ta	0.01	0.04	0.02	0.09	0.07	0.11	0.05	bd	bd	2.73	1.61	1.83	1.90	1.83	0.07	0.10	bd
Hf	0.89	0.89	1.16	1.50	2.41	1.61	0.88	0.88	0.75	1.51	1.56	1.46	1.34	1.41	0.95	0.83	0.62
La	20.71	20.76	20.43	6.73	9.05	6.88	2.35	2.24	2.11	10.10	12.00	9.94	10.29	10.35	3.14	3.02	3.32
Ce	70.19	69.42	70.24	22.41	28.93	21.65	6.61	6.27	6.37	30.73	35.51	27.40	27.48	27.49	8.41	8.98	9.10
Pr	10.64	10.14	10.23	3.73	4.15	3.22	1.05	0.90	0.99	4.71	4.74	4.04	4.14	4.25	1.29	1.40	1.27
Nd	46.37	49.40	44.52	18.45	19.25	15.56	5.81	5.42	5.63	21.61	24.53	19.82	20.19	19.78	7.03	6.86	7.19
Sm	8.61	8.91	8.29	5.64	5.50	3.61	1.84	1.81	2.07	5.89	5.61	5.08	5.55	5.07	2.59	2.21	2.45
Eu	2.14	2.15	2.18	1.75	1.79	1.42	0.71	0.66	0.65	2.04	1.90	1.78	1.94	2.04	0.89	0.80	0.75
Gd	5.74	5.11	5.48	4.99	4.84	3.47	2.58	1.92	2.46	5.50	5.61	4.56	4.31	4.64	2.43	2.81	2.77
Tb	0.80	0.72	0.75	0.72	0.90	0.58	0.43	0.39	0.42	0.89	0.78	0.71	0.72	0.70	0.45	0.54	0.56
Dy	3.60	3.36	3.60	4.81	5.16	4.02	3.25	2.67	2.76	4.30	4.14	4.17	4.29	4.66	3.21	2.97	2.88
Ho	0.68	0.57	0.66	0.97	1.06	0.71	0.67	0.58	0.56	0.91	0.88	0.88	0.97	0.92	0.56	0.75	0.69
Er	1.86	1.72	1.67	2.20	2.71	2.00	1.98	1.70	1.55	2.18	2.25	2.18	2.45	2.22	1.76	1.98	2.00
Tm	0.27	0.22	0.20	0.27	0.39	0.25	0.30	0.29	0.24	0.26	0.33	0.33	0.32	0.32	0.27	0.30	0.22
Yb	1.44	1.43	1.38	2.00	2.52	1.80	1.83	1.74	1.95	2.11	1.56	2.16	2.54	1.86	1.57	2.37	1.61
Lu	0.18	0.20	0.17	0.26	0.39	0.27	0.26	0.26	0.24	0.22	0.28	0.31	0.31	0.28	0.29	0.24	0.22
LREE	156.52	158.63	153.71	56.96	66.88	50.92	17.65	16.64	17.17	73.05	82.39	66.28	67.65	66.94	22.47	22.48	23.32
HREE	14.56	13.34	13.91	16.21	17.96	13.10	11.30	9.54	10.17	16.36	15.84	15.30	15.90	15.59	10.54	11.95	10.95
REE	173.22	174.12	169.80	74.92	86.63	65.44	29.66	26.84	27.99	91.45	100.13	83.36	85.49	84.57	33.90	35.23	35.02

na, not analysed; bd, below detection limit.

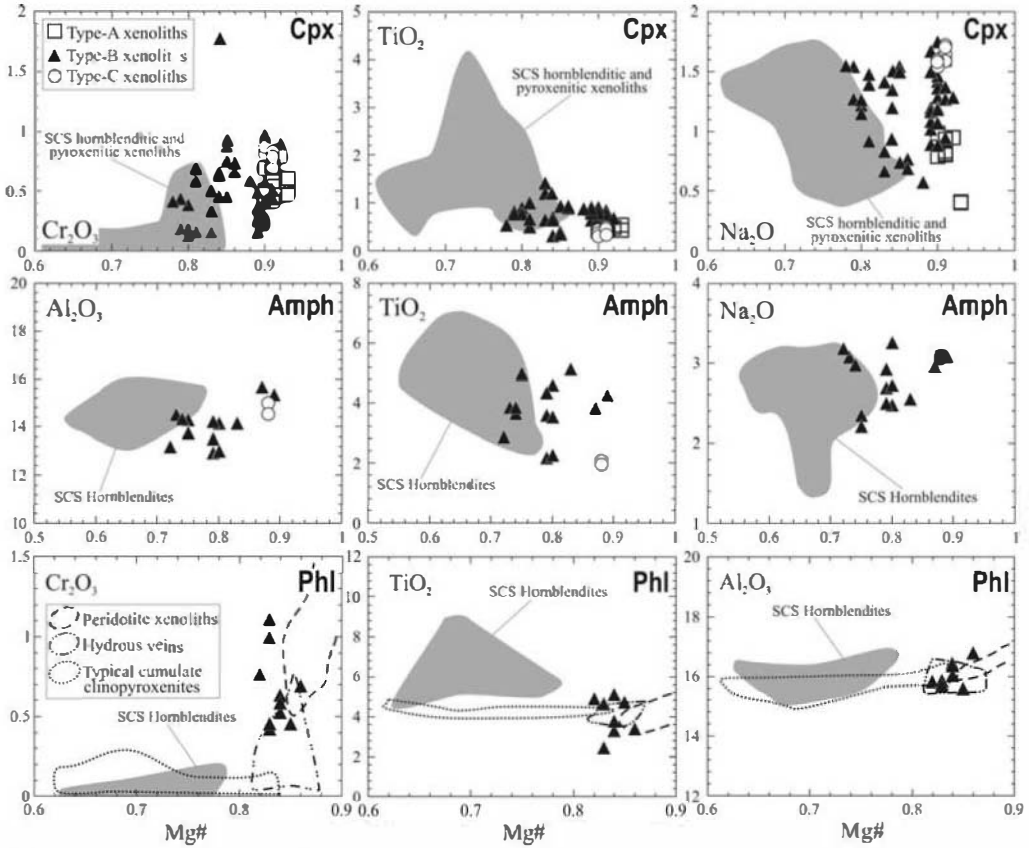

Fig. 3. Major element composition of clinopyroxene, amphibole and phlogopite from the altered ultramafic SCS xenoliths. Mineral composition of the SCS Sp-pyroxenites and hornblendites taken from Orejana *et al.* (2006). Fields of phlogopites from peridotites, hydrous veins and typical clinopyroxenites after Shaw (2004).

(1.14–2.75 ppm), Nb (0.14–1.55 ppm) and Ta (0.02–0.17 ppm) are clearly higher, whereas the converse applies to Sr (92.9–111.8 ppm) (Fig. 4b). Type B clinopyroxenes are also distinguished by their lower Cr concentration (1630–3080 ppm) when compared with type A and C clinopyroxenes (4158–5310 ppm) (Table 3). Finally, type C clinopyroxenes have generally lower trace element concentrations (Sr 40.9–44.1 ppm; Zr 15.7–18.2 ppm; Nb 0.1–0.6 ppm; LREE 16.6–17.7 ppm), with their maximum difference being the almost flat chondrite-normalized REE patterns (Fig. 4a).

Amphibole trace element compositions reproduce the chondrite- and primitive mantle-normalized patterns of clinopyroxenes in each xenolith, showing marked heterogeneity (Table 3). Type B amphiboles are characteristically LREE enriched and show a convex-upwards REE pattern, with La abundances *c.* 40 times chondrite values (Fig. 4c). This composition is similar to that of amphiboles interpreted as deep cumulates crystallized from alkaline basic melts (Irving & Frey 1984), although being LREE enriched. The primitive mantle-normalized trace element pattern of amphiboles from type B xenoliths is characterized by Ba and Nb–Ta positive peaks and U–Th and Zr–Hf negative anomalies (Fig. 4d). These patterns contrast markedly with that of amphiboles from type C xenoliths, which show general low trace element concentrations; REE have flat patterns, similar to that for clinopyroxene from these xenoliths, and primitive mantle spidergrams are characterized by the presence of high field strength elemet (HFSE) (Nb–Ta and Zr–Hf) negative anomalies (Fig. 4d).

Whole-rock geochemistry

Major and trace element composition

It has been possible to analyse only two altered ultramafic SCS xenoliths for whole-rock geochemistry.

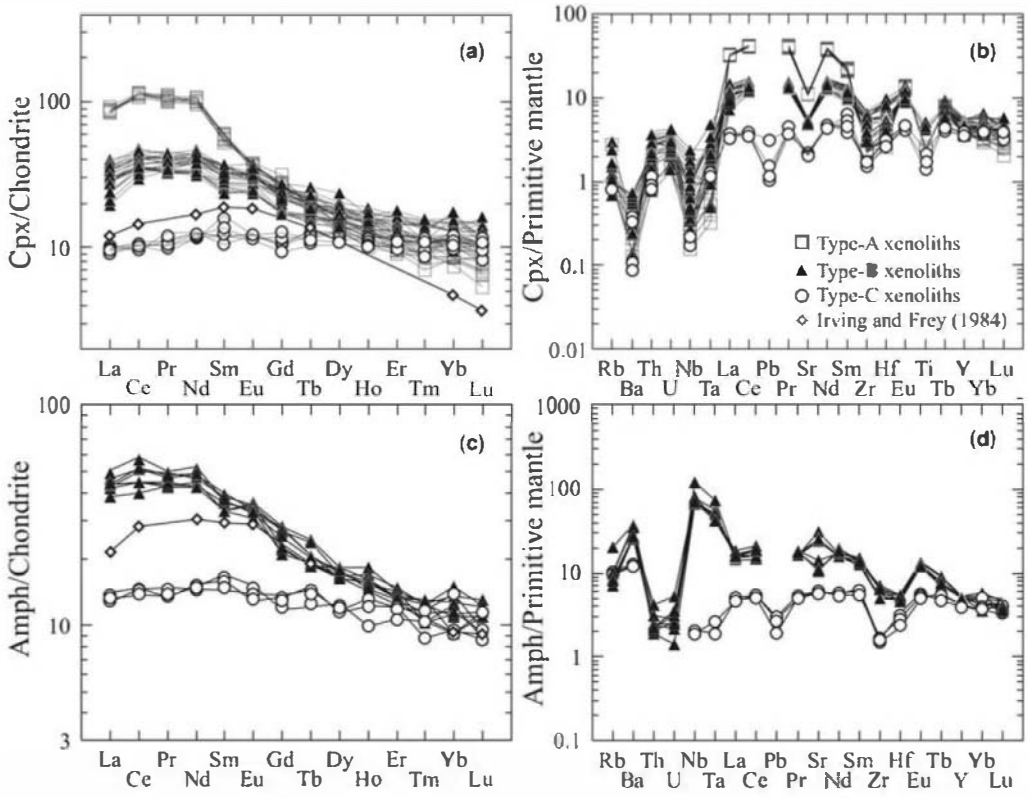

Fig. 4. (**a**) Chondrite-normalized and (**b**) primitive mantle-normalized trace element composition of clinopyroxenes from the altered ultramafic SCS xenoliths. (**c**) Chondrite-normalized and (**d**) primitive mantle-normalized trace element composition of amphiboles from the altered ultramafic SCS xenoliths. Data for other SCS xenoliths are taken from Orejana *et al.* (2006). ◆, averaged REE composition of deep cumulates from basaltic magmas, taken from Irving & Frey (1984). Chondrite and primitive mantle values are taken, respectively, from Sun & McDonough (1989) and McDonough & Sun (1995).

These two samples correspond to type A and C xenoliths. Nevertheless, major and trace element composition, as well as isotopic ratios, are necessarily influenced by their high degree of alteration (Table 1): 86.5 vol% in sample 105776 (type A xenoliths) and 78.8 vol% in sample 105787 (type C xenoliths), and their high loss on ignition (LOI) values (close to 10 wt%), so that these results should be interpreted with caution.

The major element composition of these xenoliths is characterized by low contents of TiO_2 (<0.2 wt%), CaO (<4 wt%), Na_2O (<0.47 wt%) and K_2O (<0.13 wt%), and relatively high concentrations of SiO_2 (48–50 wt%) and MgO (23–24 wt%) (Table 4). The high proportion of secondary talc in the analysed samples could explain the Si–Mg-rich nature of these altered xenoliths (Mg-number values vary from 0.81 to 0.84). The low CaO content is likely to be related to the scarcity of modal clinopyroxene (10–17%).

Both xenoliths have a homogeneous major element composition, different from those of most of the cumulate pyroxenites and hornblendites of Orejana *et al.* (2006), although they plot close to the websterite xenolith 102131 (Fig. 5). It is important to note the similarity between major element contents of the analysed altered xenoliths and the orthopyroxene composition (taken from the above-mentioned websterite 102131) (Fig. 5). The whole-rock composition of analysed pyroxenites yields high normative *Hy* for both samples (Table 4), indicating the predominance of orthopyroxene in the original modal composition of the xenoliths.

Altered ultramafic SCS xenoliths have variable trace element contents. Sample 105776 (type A) has higher REE–LILE–HFSE contents compared with sample 105787 (type C) (Table 4). On the whole, both pyroxenites show low concentrations, although some incompatible elements display moderate (Rb, K and LREE), or even high contents

Table 4. *Whole-rock geochemistry of SCS altered ultramafic xenoliths (major elements, trace elements, Sr–Nd isotope ratios and CIPW normative composition)**

	Sample				
	105776	105787		105776	105787
SiO_2	49.67	48.32	Ba	30.1	203
TiO_2	0.2	0.1	Rb	6.61	4.07
Al_2O_3	4.09	4.43	Cs	8.96	4.15
$Fe_2O_3^{\dagger}$	11.02	9.08	Sr	58.8	58.5
MnO	0.03	0.07	Pb	1.93	bd
MgO	23.07	23.85	Th	0.18	0.02
CaO	2.21	4	U	0.12	0.02
Na_2O	0.19	0.47	Zr	14.5	3.30
K_2O	0.12	0.13	Nb	2.07	0.23
P_2O_5	0.07	0	Y	7.21	3.74
LOI	9.51	9.75	V	89.4	91.1
Total	100.18	100.2	Ni	1910	2117
Mg-no.	0.81	0.84	Cr	2948	3043
			Ta	0.15	0.02
Q	2.9	0.0	Hf	0.44	0.14
Or	0.8	0.9	La	7.09	2.45
Ab	1.8	4.4	Ce	10.22	5.91
An	11.1	10.7	Pr	1.39	0.74
Ne	0.0	0.0	Nd	5.94	2.93
Lc	0.0	0.0	Sm	1.40	0.65
Di	0.6	9.1	Eu	0.50	0.23
Hy	79.8	66.0	Gd	1.41	0.66
Ol	0.0	6.7	Tb	0.24	0.11
Mt	2.4	2.0	Dy	1.37	0.67
Il	0.4	0.2	Ho	0.26	0.14
Ap	0.2	0.0	Er	0.73	0.38
End-members			Tm	0.11	0.06
Ol	0.0	8.2	Yb	0.70	0.35
Hy	99.3	80.7	Lu	0.11	0.06
Dy	0.7	11.1			
Sr–Nd isotopic ratios					
$^{87}Rb/^{86}Sr$	0.32	0.2	$^{147}Sm/^{144}Nd$	0.1426	0.1341
$^{87}Sr/^{86}Sr \pm 2\sigma$	0.707811 ± 47	0.707800 ± 05	$^{143}Nd/^{144}Nd \pm 2\sigma$	0.512597 ± 06	0.512585 ± 06
$^{87}Sr/^{86}Sr_{265Ma}$	0.70658	0.70704	$\varepsilon(Nd)_{265\ Ma}$	1.03	1.08

*Normative composition has been calculated considering that Fe_2O_3 represents 15% of total Fe.
†Total Fe is represented as Fe_2O_3.
bd, below detection limit.

(Ba in sample 105787, 203 ppm). The chondrite-normalized REE pattern is flat for HREE and increasingly fractionated from middle REE (MREE) to LREE, and is subparallel for the two samples (Fig. 6a). The primitive mantle-normalized trace element patterns display clear negative anomalies for HFSE (Th, Nb–Ta, Zr–Hf and Ti), but they are significantly more marked in sample 105787 (type C) than in sample 105776 (type A) (Fig. 6b). In this latter xenolith, whole-rock trace element geochemistry is dominated by clinopyroxene composition, and the normalized patterns mimic those of this mineral, with negative anomalies at the HFSE. A similar pattern occurs for sample 105787, where the presence of a HFSE-poor amphibole adds to the HFSE-poor nature of clinopyroxene, although it results in the increased Ba concentration of this xenolith.

Sr–Nd isotope composition

The initial Sr and Nd isotopic ratios of the analysed altered ultramafic SCS xenoliths have $(^{87}Sr/^{86}Sr)_0$

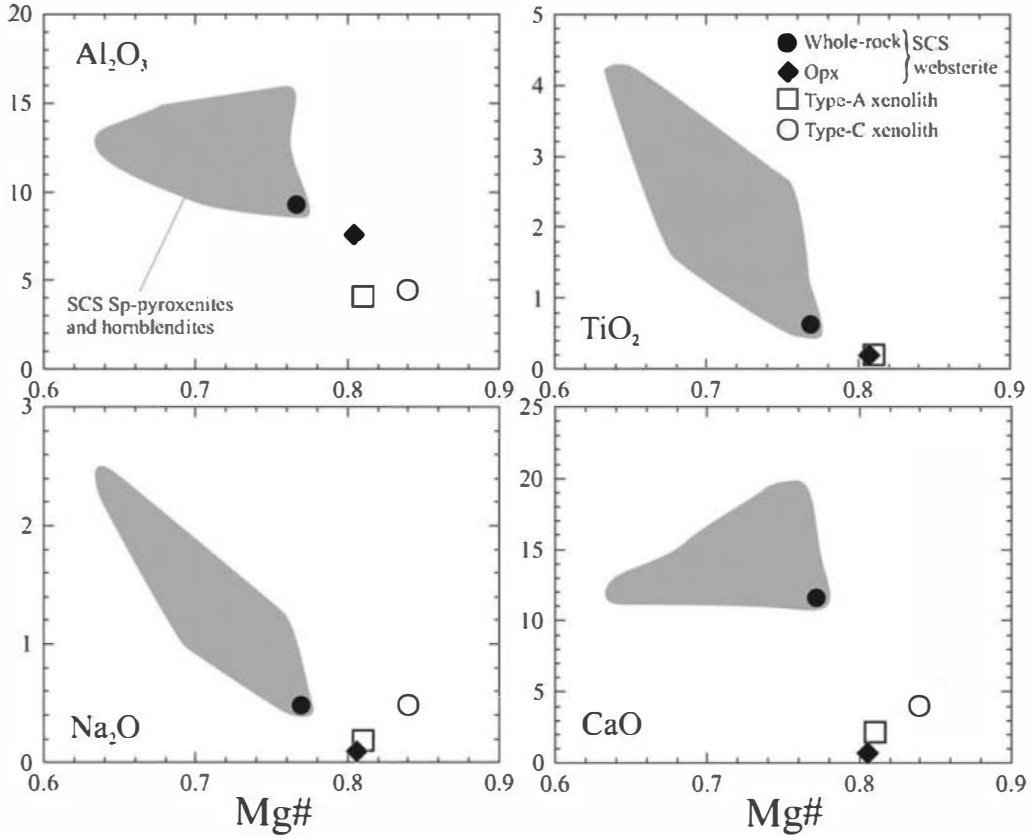

Fig. 5. Major element whole-rock composition of the altered ultramafic SCS xenoliths. Fields of other ultramafic SCS xenoliths (Sp-pyroxenites and hornblendites) and whole-rock and orthopyroxene composition of the websterite 102131 are taken from Orejana *et al.* (2006).

from 0.70658 to 0.70704 and εNd *c.* +1 (Table 4). The Sr isotopic composition of the host dykes is markedly different from that of the altered xenoliths, but radiogenic Nd values resemble those of the isotopically enriched lamprophyre dykes, and also those of the more radiogenic subalkaline SCS pyroxenites (Fig. 7). This composition falls outside the mantle array, because of the relative

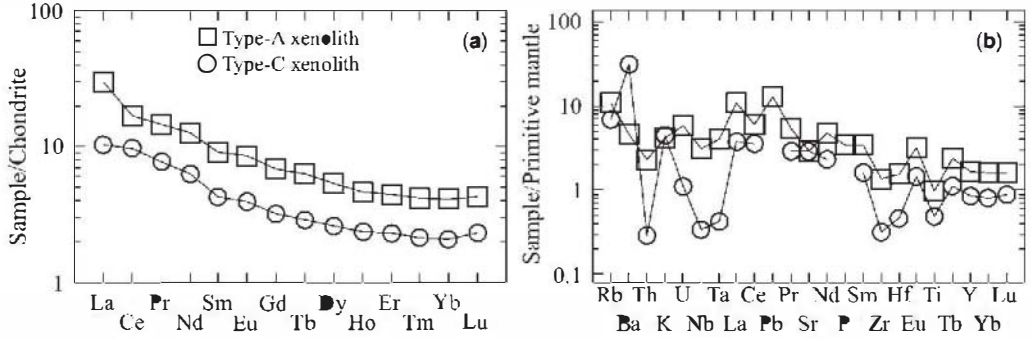

Fig. 6. (a) Chondrite-normalized and (b) primitive mantle-normalized trace element composition of the altered ultramafic SCS xenoliths. Normalizing values for chondrite and primitive mantle from Sun & McDonough (1989) and McDonough & Sun (1995), respectively.

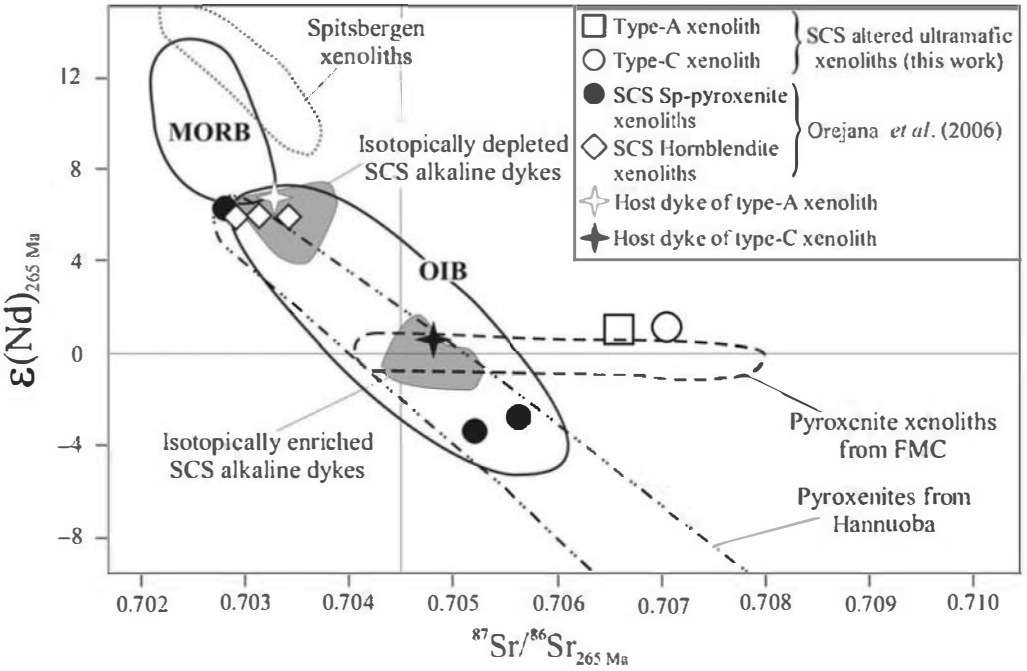

Fig. 7. Sr–Nd isotopic composition of altered xenoliths (calculated at 265 Ma), in comparison with isotopic ratios of the SCS alkaline magmatism (Villaseca *et al.* 2004), SCS cumulate pyroxenites (Orejana *et al.* 2006) and pyroxenite xenoliths from the FMC (Downes & Dupuy 1987), Spitsbergen (Ionov *et al.* 2002*b*) and Hannuoba (Xu 2002). MORB and OIB fields are after Wilson (1989).

radiogenic Sr, whereas εNd values are similar to BSE (Bulk Silicate Earth) values. Similar deviations from the mantle array have been described in mantle xenoliths from Spitsbergen (Ionov *et al.* 2002*b*) and the French Massif Central (FMC) (Downes & Dupuy 1987) (Fig. 7), and have been interpreted as a consequence of percolative porous melt flow metasomatism and an enrichment event caused by EMI-like magmas, respectively. This high $^{87}Sr/^{86}Sr$ trend of the altered SCS xenoliths contrasts with that displayed by pyroxenite xenoliths from Hannuoba (towards both higher Sr and lower Nd radiogenic ratios), which might represent the involvement of fluids derived from subduction or from a delaminated lower crust (Xu 2002).

Discussion

The origin of secondary alteration

The presence of chlorite and talc in these xenoliths suggests re-equilibration in a volatile-rich environment, probably interacting with a H_2O–CO_2-rich fluid. The selective alteration, which mainly affects the primary orthopyroxene of the xenolith, is also reproduced in the host lamprophyre where clinopyroxene, amphibole or phlogopite phenocrysts are well preserved, whereas olivine is totally pseudomorphed by talc. The common presence of carbonate-rich and chlorite-rich ocelli in the lamprophyres suggests significant volatile exsolution by the ultrabasic magma at subvolcanic emplacement levels. Thus, it is possible that a selective low-*P* alteration of suspended solids (xenoliths, phenocrysts) occurred during lamprophyric magma devolatilization. Chlorite group minerals in ultramafic assemblages can appear at high temperatures under low-pressure conditions (<1 kbar), in the range of 850–900 °C (Pawley 2003). Talc could appear slightly later, at around 800 °C (Pawley & Wood 1995). This estimate of relatively high-temperature alteration is close to, or overlaps, the solidus condition for volatile-rich lamprophyric magmas (Esperança & Holloway 1987). Volatiles exsolved from the lamprophyric melt react with suspended solids (xenoliths, phenocrysts) and promote the alteration of a restricted mineral phase assemblage (i.e. orthopyroxene in pyroxenites, garnet in granulite xenoliths and olivine in lamprophyres). The restricted alteration of pyroxenite xenoliths (not related to vein or fracture filling) and olivine

in lamprophyres could continue to late-stage or subsolidus conditions. The subsolidus autometasomatic alteration of primary minerals in lamprophyres as a result of their high volatile content has been frequently described (Rock 1991). Petrographic features also do not suggest external hydrothermal invasive alteration, in agreement with the anorogenic setting of this alkaline magmatism. Devolatilization of the lamprophyric magma is the only possible agent to alter the incorporated xenoliths close to or at the shallow level of emplacement.

Nature of the metasomatic agents

The presence of high-*P* and high-*T* metasomatism within the altered SCS pyroxenite xenoliths can be recognized in the formation of new minerals (mainly Mg–Cr-rich amphibole and phlogopite) and in the modification of the incompatible trace element composition of the clinopyroxene (and more specifically LREE enrichment and variable HFSE depletion). The major element composition of studied amphibole and phlogopite is very similar to that shown by equivalent phases interpreted as the products of metasomatism within mantle xenoliths (Ionov *et al.* 1997). Amphiboles are essentially Ti–Cr-pargasites (less commonly kaersutites) and micas are titanian phlogopites. In all samples the Mg-number values of amphibole and mica are very close to those of coexisting clinopyroxene (Table 2), indicating that the minerals are close to chemical equilibrium. Type A and C altered SCS xenoliths show a homogeneous mineral composition, with Mg-number in the narrow range 0.88–0.93 for both amphibole and clinopyroxene. Greater heterogeneity in major element mineral chemistry is shown by type B xenoliths, but they also display similar Mg-number for their constituent minerals (0.78–0.92 for clinopyroxene, 0.72–0.89 for amphibole and 0.82–0.86 for phlogopite).

The most significant differences between the altered SCS xenoliths are mainly restricted to trace element mineral compositions. Type A xenoliths do not show hydrous high-T minerals (amphibole or phlogopite) indicative of modal metasomatism, but clinopyroxene displays highly LREE-enriched chondrite-normalized patterns (Fig. 4a), with high $(La/Yb)_N$ ratios ranging from 7.8 to 11.6 (Fig. 8). Moreover, strong negative HFSE (Nb–Ta, Zr–Hf and Ti) anomalies and high concentrations of Sr may be recognized (Fig. 4b). These characteristics indicate the involvement of cryptic metasomatism, which is analogous to similar enrichment in peridotite xenoliths from basalts (e.g. Frey & Prinz 1978; Kempton 1987; Kempton *et al.* 1999).

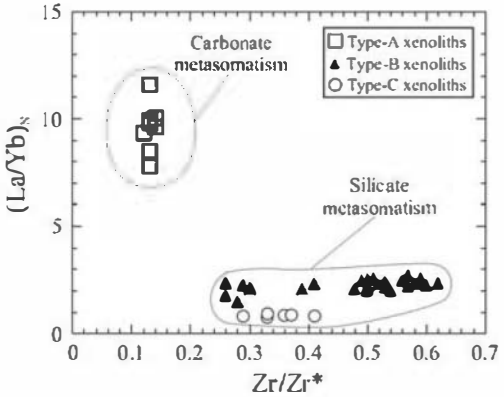

Fig. 8. $(La/Yb)_N$ v. Zr anomaly ($Zr/Zr^* = Zr_N/(Eu_N + ((Sm_N - Eu_N)/2))$) for clinopyroxene from the altered ultramafic SCS xenoliths.

Strong enrichments in LREE have been related to silicate and carbonate melts (Downes 2001; Ionov *et al.* 2002*a*; Xu 2002; Xu *et al.* 2003). Experimental studies on carbonate metasomatism have concluded that carbonatite melts may carry high concentrations of LILE, REE, U and Th, but they are characterized by low HFSE contents (Green & Wallace 1988). This HFSE depletion leads to the formation of clinopyroxene with deep troughs at Ta–(Nb), Zr–Hf and Ti, if a carbonate melt acts as the metasomatic agent (e.g. Ionov 1998; Yaxley *et al.* 1998). The above premises coincide with the $(La/Yb)_N$ and Zr/Zr^* values, which have been used to distinguish between clinopyroxenes associated with carbonate and silicate metasomatism (Fig. 8). We have calculated the composition of melts in equilibrium with type A clinopyroxenes using the cpx/carbonatite partition coefficients of the compilation of Klemme *et al.* (1995). The results represent liquids with a composition very similar to the average composition of calciocarbonatites (Woolley & Kempe 1989) or to that of selected Kola carbonatites (Downes *et al.* 2005) (Fig. 9a), suggesting that a carbonate-rich melt was likely to have been responsible for the cryptic metasomatism in type A xenoliths.

Type B xenoliths contain clinopyroxene and amphibole with convex-upwards chondrite-normalized REE patterns, resembling those of deep-seated cumulates from basaltic magmas (Irving & Frey 1984), but they are markedly more LREE-rich, with the peak position normally located at Ce (Fig. 4a). Amphibole is characteristically enriched in Nb–Ta and Ti (Fig. 4d), which is typical of Mg–Cr-rich metasomatic amphiboles crystallized in veins within the mantle from highly alkaline basic melts (Downes 2001; Witt-Eickschen *et al.*

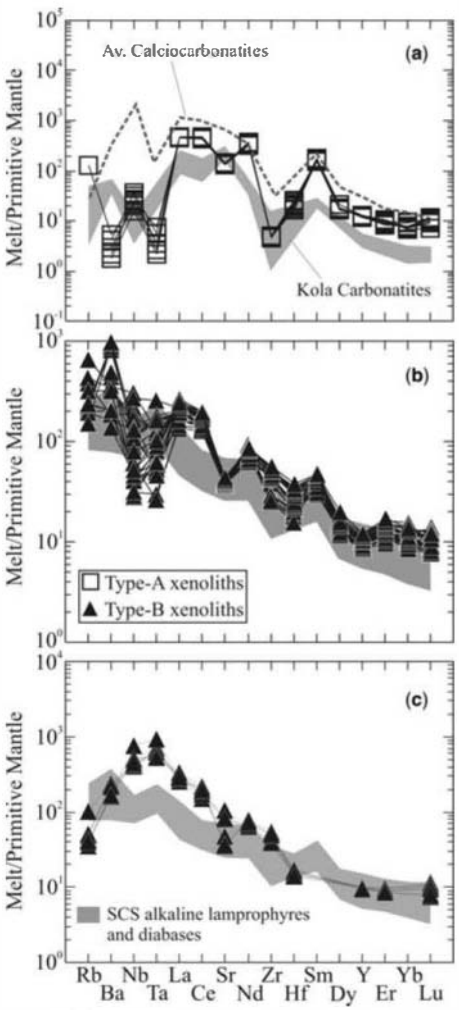

Fig. 9. (**a**) Trace element composition of melts in equilibrium with clinopyroxenes from type A altered xenoliths, associated with carbonate melts. Data calculated using cpx/carbonatite melt partition coefficients (Klemme *et al.* 1995). (**b**) Trace element composition of melts in equilibrium with clinopyroxenes from type B altered xenoliths, associated with the SCS alkaline magmas. Data calculated using cpx/basaltic melt partition coefficients (Hart & Dunn 1993), except for Rb (Foley *et al.* 1996) and Ta (averaged value determined at $P = 1.0$ GPa by Skulski *et al.* 1994). (**c**) Trace element composition of melts in equilibrium with amphiboles from type B altered xenoliths, associated with the SCS alkaline magmas. Data calculated using amph/silicate melt partition coefficients of LaTourrette *et al.* (1995). Average composition of calciocarbonatites taken from Woolley & Kempe (1989). Compositional field of selected Kola carbonatites taken from Downes *et al.* (2005). SCS alkaline dykes range taken from Villaseca *et al.* (2004). Normalizing values for primitive mantle from McDonough & Sun (1995).

2003). Phlogopite is also typically Cr–Mg-rich, displaying higher Mg-number (0.82–0.86) and lower TiO_2 contents (<5 wt%) than those expected for micas formed from evolved basic melts as pyroxenitic xenoliths (Mg-number *c.* 0.65–0.75 and TiO_2 *c.* 6–9 wt%; Ionov *et al.* 1997; Shaw 2004), whereas Cr and Mg concentrations resemble those of metasomatic micas crystallized in veins within the upper mantle (Fig. 3). Trace element signatures of clinopyroxene and amphibole from type B xenoliths point clearly to a metasomatic origin associated with an alkaline silicate melt (modal metasomatism). Using the experimental cpx/silicate melt partition coefficients of Hart & Dunn (1993), except for Rb (Foley *et al.* 1996) and Ta (averaged value determined at $P = 1.0$ GPa by Skulski *et al.* 1994), and the amph/silicate melt partition coefficients of LaTourrette *et al.* (1995), we have calculated the hypothetical trace element composition of melts in equilibrium with both minerals from this type of xenolith, which is represented in Figure 9b and c. The primitive mantle-normalized trace element pattern of estimated melts broadly overlaps the compositional range corresponding to the SCS Permian alkaline lamprophyres and diabases, only showing slightly higher concentrations of Nb, Ta, La and Ce for estimates made using $D^{amph/melt}$. This similarity suggests that the metasomatic agent responsible for the crystallization of amphibole and the modification of the clinopyroxene trace element composition from type B xenoliths might be genetically related to the SCS Permian alkaline magmatism.

The third distinctive geochemical signature described in the altered ultramafic SCS xenoliths corresponds to clinopyroxene and amphibole from type C xenoliths, which display similar flat REE patterns and strong HFSE depletions. This latter aspect contrasts significantly with the primitive mantle-normalized trace element patterns of amphiboles from type B and C xenoliths: the former gives rise to strong positive Nb–Ta anomalies, whereas type C amphiboles show negative Nb–Ta anomalies (Fig. 4d). In contrast, the HFSE depletions in clinopyroxenes from type A and C xenoliths (Fig. 4b) represent analogous behaviour indicative of high incompatibility of these elements in both metasomatizing agents, and, in general terms, this characteristic has been ascribed to reaction with H_2O–CO_2-rich melts (e.g. Downes 2001; Ionov *et al.* 2002a; Xu & Bodinier 2004).

Single or multiple enrichment events?

The heterogeneous trace element mineral chemistry of the altered SCS xenoliths can be explained by advocating two possibilities: (1) that different,

genetically unrelated metasomatic agents have operated within the upper mantle–lower crust boundary below the SCS, giving rise to three contrasting trace element patterns; or (2) that a single melt has affected the wall-rock after fractionating to produce three different (but genetically linked) metasomatic agents. In any case, the composition of melts in equilibrium with type B xenoliths strongly supports metasomatism being caused by highly alkaline magmas similar to the SCS Late Permian alkaline magmatism, which is the only alkaline magmatic event recorded in central Spain.

There are numerous cases where heterogeneous trace element enrichment signatures within mantle xenoliths have been interpreted as being controlled by a unique metasomatic agent, as a result of a differentiation process (e.g. Grégoire *et al.* 2000; Xu & Bodinier 2004). Opposite to modal metasomatism within the wall-rock, restricted to zones adjacent to vein conduits, a 'diffuse' metasomatism has been proposed, corresponding to migrations of melts that percolate along grain boundaries in a solid matrix (i.e. porous flow; e.g. Xu & Bodinier 2004). The metasomatic agent is generally a small melt fraction rich in volatiles. Such melts, because of their low viscosity and low dihedral wetting angles, such as occur for carbonatitic melts, can escape their source regions at melt fractions as low as 0.1%, percolating through the rock matrix because of the formation of interconnected grain-edge networks (e.g. Minarik 1998; Witt-Eickschen *et al.* 2003). This characteristic makes these magmas very effective as mobile metasomatic agents in the lithospheric mantle (Navon & Stolper 1987; Green & Wallace 1988; Yaxley *et al.* 1998). Reactive porous flow metasomatism has been used to explain the variable LREE enrichment in clinopyroxene with almost constant HREE (Bedini *et al.* 1997; Vernières *et al.* 1997; Ionov *et al.* 2002*a*). Moreover, a direct relationship between the style of metasomatism and the distance from its source has been observed in peridotite massifs (e.g. Bodinier *et al.* 1990), and ascribed to a single metasomatic event involving a progressively differentiated melt solidifying down a thermal gradient. Nevertheless, the general equilibrium conditions attained by minerals in the altered SCS xenoliths, as demonstrated by similar Mg-number values and the absence of strongly fractionated LREE ratios, such as La/Ce, La/Pr or La/Nd, suggest that source composition dominated the metasomatic process over fractionation mechanisms (chromatographic effect), so that the rock acquired strong chemical fingerprints of the metasomatic agents.

We propose that metasomatism within the altered ultramafic SCS xenoliths represents the involvement of a single parental melt. The estimated trace element composition of melts in equilibrium with type B xenoliths (associated with silicate melt metasomatism) suggests that this agent was similar to the Permian alkaline magmatism. Clinopyroxene and amphibole from type B xenoliths show chemical characteristics similar to those of metasomatic phases crystallized in veins. Nevertheless, a differentiation process must have occurred while alkaline melts percolated through the wall-rock, to produce type A–C geochemical signatures. Crystallization of amphibole and phlogopite in vein conduits and in the wall-rock may result in a significant decrease in water and Nb–Ta contents in the residual melts. Taking into account the high H_2O and CO_2 contents characteristic of these alkaline melts, a decrease in water in the percolating fluid or melt would favour the formation of a carbonate-rich fraction responsible for the anhydrous transformation of type A xenoliths, probably at a greater distance from the magma source. Reaction of a carbonate melt with the wall-rock would result in a continuous exhaustion of its silicate component and an increasing proportion of the carbonate component in its composition (Mattielli *et al.* 1999), because carbonates are not stable in the shallow mantle at moderate to high temperatures (Dalton & Wood 1993).

Formation of type C clinopyroxene and amphibole may be interpreted within this theoretical model. The differences shown by type B and type C amphiboles in their trace element composition (e.g. Zr–Nb concentrations) are very similar to those described for vein and disseminated amphiboles within metasomatized mantle xenoliths (Ionov *et al.* 1997; Fig. 10). Whereas convex-upwards REE patterns in type B xenoliths could be ascribed to silicate melt crystallization in veins, the flat REE patterns and the negative HFSE anomalies of

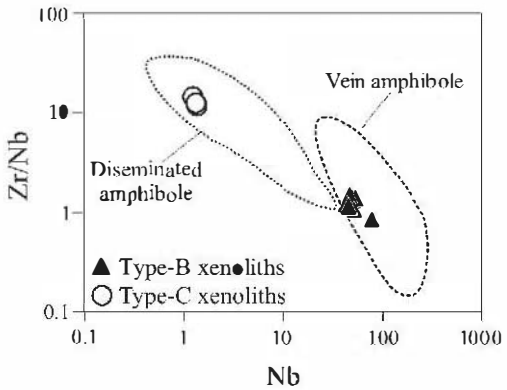

Fig. 10. Zr/Nb v. Nb for amphiboles from the altered ultramafic SCS xenoliths. Fields for disseminated and vein amphibole are taken from Ionov *et al.* (1997).

amphibole from type C xenoliths resemble trace element contents of disseminated amphibole. Transition from the convex-shaped REE pattern to the LREE-depleted pattern for vein and disseminated amphiboles, respectively, has been documented in several studies (Downes *et al.* 1995; Vaselli *et al.* 1995; Zanetti *et al.* 1996). The above differences in trace element composition between metasomatic amphiboles have been explained by the lower solubility of HFSE in aqueous fluids when compared with silicate melts (Ionov & Hofmann 1995), in accordance with the widely accepted model of mantle metasomatism involving expulsion of fluids from a network of veins filled with crystallizing basaltic melts (Wilshire 1987; O'Reilly *et al.* 1991). Thus, it is likely that percolation of the H_2O–CO_2-rich metasomatic agent, before total exhaustion of water, would have given rise to crystallization of a HFSE-poor amphibole in type C xenoliths.

Nature of the pyroxenite protolith

Although the whole-rock geochemistry of type B xenoliths has not been determined, the similarities in petrography (granoblastic texture, high degree and type of alteration, modal composition), and in major element mineral composition, when compared with the other altered xenoliths, suggest that they all are probably related to similar protoliths. The modal abundance of pseudomorphed orthopyroxene, as stated above, combined with their Opx-rich normative composition (Table 4) and the negative Nb–Ta (immobile elements) anomaly in multi-element normalized plots shown by the pyroxenites are in clearly contrast to the host alkaline magma chemistry. Subsequently, pyroxenite parental melts show a sub-alkaline affinity. Their granoblastic texture indicates solid-state equilibration before being trapped by ascending alkaline magmas.

P–T estimates on mineral equilibria in ultramafic xenoliths give metamorphic conditions close to mantle–crust boundary levels (Orejana *et al.* 2006). This is in agreement with estimated conditions for accompanying granulite xenoliths (Villaseca *et al.* 1999). Moreover, recent estimates on pyroxene-bearing chamockite xenoliths also yield *P–T* conditions that rarely indicate significant mantle depths, taking into account an estimated average crustal thickness of 35km (see Villaseca *et al.* 1999, and references therein). *P–T* estimates in the studied altered pyroxenites using single-cpx thermometry (Mercier 1980), Ti-in-amphibole thermometry (Otten 1984) and cpx barometry (Nimis & Ulmer 1998) give values that are mostly in the range of 935–1075 °C and 7.6–10.2 kbar (Table 2), overlapping previously published data on SCS xenolith suites. The lack of clear mantle-derived (i.e. peridotite) xenoliths in the lamprophyres also argues for a non-mantle provenance of these rocks. Thus, pyroxenite xenoliths could represent ultramafic igneous bodies recrystallized during granulite-facies conditions at the base of the SCS continental crust.

Prior to entrainment of the alkaline magmatism, three intrusive suites of calc-alkaline basic rocks have been identified within the SCS (Villaseca *et al.* 2004): (1) gabbros to quartz diorites emplaced in small massifs (Gb1), coeval with the granitic Hercynian batholith; (2) medium-K calc-alkaline dyke swarms (Gb2); (3) shoshonitic dyke swarms (Gb3). Gb1 rocks were intruded between 345 and 310Ma (Bea *et al.* 1999), whereas Gb2 and Gb3 represent a post-collisional, late-stage magmatism emplaced no earlier than 295Ma (Galindo *et al.* 1994). Thus, the origin of the protolith of the altered SCS xenoliths might be associated with crystallization of ultramafic pyroxene-rich cumulates from these basic sub-alkaline magmas at the lower crust–upper mantle boundary, in the context of an underplating event, as has been proposed for other Permian pyroxenitic xenoliths from the French Massif Central (Féménias *et al.* 2003).

The Sr–Nd isotopic ratios (calculated at 265Ma) of the two analysed samples (type A and C xenoliths) give rise to a homogeneous εNd *c.* +1, but relatively variable radiogenic Sr isotopic ratios (Fig. 11). A wide range of $^{87}Sr/^{86}Sr$ ratios in ultramafic xenoliths accompanied by little variation of the εNd value has been explained by interaction with oceanic waters associated with a lithospheric component affected by subduction (e.g. Downes *et al.* 1992; Rosenbaum *et al.* 1997; Downes 2001; Xu 2002). Nevertheless, the SCS represents the innermost part of the Hercynian Belt, precluding the possibility of an oceanic subducted component in this region. Moreover, the primary mineral chemistry of the altered SCS xenoliths strongly suggests that metasomatism was caused by the infiltration of alkaline magmas genetically related to the host Permian alkaline dykes. Superimposed upon this there is also a later strong alteration process caused by the devolatilization of the lamprophyric magma.

The relatively enriched Sr isotopic signature might represent an enriched composition in the source, probably linked to the Gb2 or Gb3 sub-alkaline basic magmas mentioned above, as they show a similar Sr isotopic composition to that of the altered xenoliths. The relatively high εNd value of the altered xenoliths points to the isotopically depleted SCS alkaline dykes as the main metasomatic melt via the two processes indicated above. We have tested this possibility by applying a simple mixing model that considers the averaged composition of the SCS depleted lamprophyres and

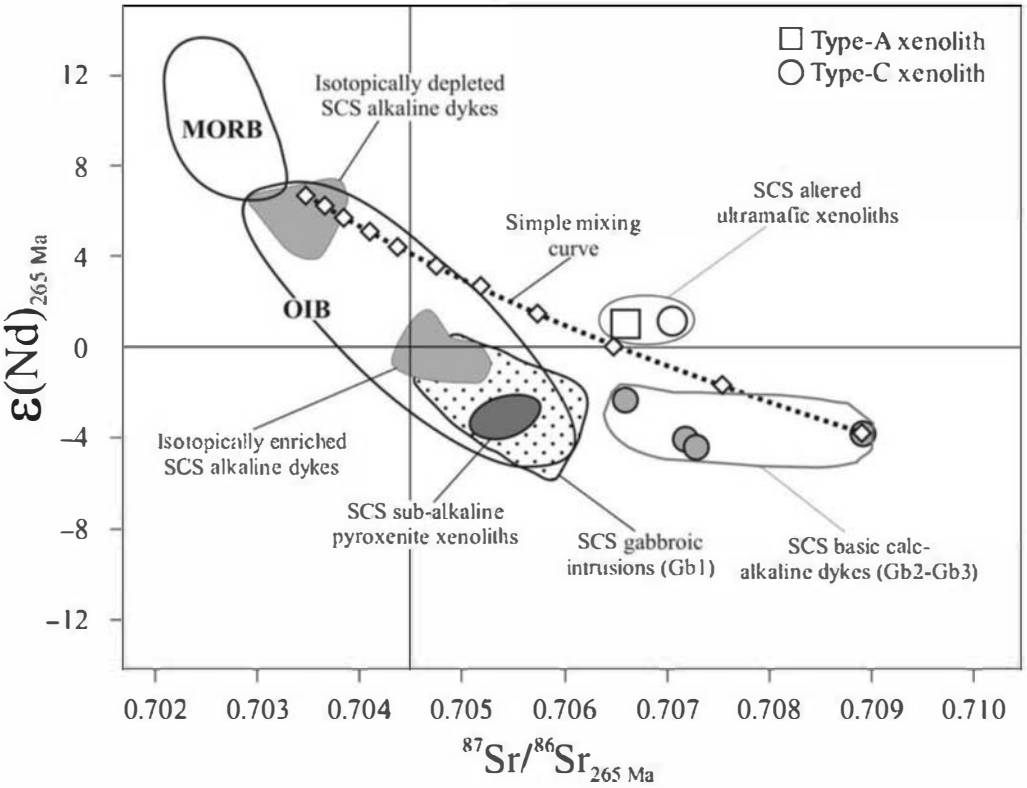

Fig. 11. Comparison of Sr–Nd isotopic ratios of the altered SCS xenoliths with respect to different SCS magmatic rocks. Composition of alkaline and sub-alkaline (Gb1–Gb2–Gb3) intrusions after Villaseca *et al.* (2004), calculated at 265 Ma. SCS sub-alkaline pyroxenitic xenoliths taken from Orejana *et al.* (2006). The curve joining small open diamonds represents a simple mixing model illustrating the probable influence of the infiltration of alkaline magmas (metasomatism and alteration) within an isotopically enriched pyroxenitic protolith. The mixing model considers the most radiogenic Gb2 sample as the starting composition $^{87}Sr/^{86}Sr = 0.70917$; $^{143}Nd/^{144}Nd = 0.512087$; Sr 230 ppm; Nd 16 ppm) and the isotopically depleted alkaline host dykes as the main metasomatic agent ($^{87}Sr/^{86}Sr = 0.70350$; $^{143}Nd/^{144}Nd = 0.512637$; Sr 800 ppm; Nd 40 ppm). MORB and OIB fields after Wilson (1989). The model suggests that metasomatism (including alteration) might be caused by the involvement of around 20% of the alkaline component.

diabases as a metasomatic melt, and a Gb2-like composition as the original calc-alkaline pyroxenitic protolith (Fig. 11). The trend described by this model predicts an isotopic modification with a 20% contribution of an alkaline melt component to explain the isotopic composition of the altered ultramafic SCS xenoliths.

Conclusions

The altered ultramafic SCS xenoliths show recrystallization textures, indicating solid-state equilibrium at the lower crustal depths. The host lamprophyric dykes do not show significant hydrothermal alteration. Thus, the secondary phases (chlorite and talc group minerals) present in the ultramafic xenoliths might have formed as a result of selective transformation, mainly of orthopyroxene, as a consequence of volatile exsolution from the host melt. The presence of unaltered clinopyroxene, amphibole and phlogopite phenocrysts in the alkaline dykes suggests that these phases should have been preserved in the xenoliths, if present. The absence of olivine and the predominance of modal clinopyroxene or normative *Hy* and *Di* indicate that these xenoliths were not mantle fragments, but represent cumulate pyroxenites of calc-alkaline affinity.

The presence of Cr–Mg-rich high-*T* hydrous phases (amphibole and phlogopite) indicates significant modal metasomatism at depth. This metasomatic process seems to be heterogeneous, as these xenoliths show three mineral trace element

signatures: type A xenoliths, with LREE-enriched clinopyroxenes with negative HFSE anomalies; type B xenoliths, with clinopyroxenes and amphiboles with high incompatible trace element contents (LILE, HFSE and REE); type C xenoliths, with relatively REE- and HFSE-poor clinopyroxenes and amphiboles. These metasomatic characteristics support crystallization from three different metasomatic agents: carbonated magma, silicate magma and hydrous fluids–melts, respectively, which are derived from the progressive differentiation of a single CO_2–H_2O-rich highly alkaline melt, genetically related to the SCS Permian alkaline lamprophyric magmatism.

The homogeneous Sr–Nd isotopic ratios of the altered xenoliths, together with their sub-alkaline nature, indicate that they formed as pyroxene-rich cumulates, associated with the intrusion of calc-alkaline basic magmas at the base of the crust during an underplating event. The radiogenic Sr composition could be explained by infiltration of an isotopically depleted melt (similar to the depleted SCS alkaline dykes) by an $^{87}Sr/^{86}Sr$-enriched component similar to Gb2 SCS calc-alkaline dykes.

We acknowledge A. F. Larios and J. G. del Tánago for their assistance with the electron microprobe analyses in the CAI of Microscopía Electrónica (UCM); also B. A. Paterson for his collaboration with laser ablation microanalysis at the Department of Earth Sciences of the University of Bristol (UK), and J. M. F. Pérez and J. A. H. Jiménez from the CAI of Geocronología y Geoquímica (UCM) for their help in analysing samples by TIMS. The detailed revision by J. M. Cebriá and G. Ceuleneer greatly increased the quality of the manuscript. We are also indebted to G. Rogers for his revision of the English. This work is included in the objectives of, and supported by, the CGL-2004-02515 project of the Ministerio de Educación y Ciencia of Spain.

References

ALLÈGRE, C. J. & TURCOTTE, D. L. 1987. Implications of a two-component marble-cake mantle. *Nature*, **323**, 123–127.

BEA, F., MONTERO, P. & MOLINA, J. F. 1999. Mafic precursors, peraluminous granitoids, and late lamprophyres in the Avila batholith; a model for the generation of Variscan batholiths in Iberia. *Journal of Geology*, **107**, 399–419.

BEDINI, R. M., BODINIER, J. L., DAUTRIA, J. M. & MORTEN, L. 1997. Evolution of LILE-enriched small melt fractions in the lithospheric mantle: a case study from the East Africa Rift. *Earth and Planetary Science Letters*, **153**, 67–83.

BODINIER, J. L., VASSEUR, G., VERNIÈRES, J., DUPUY, C. & FABRIÉS, J. 1990. Mechanisms of mantle metasomatism: geochemical evidence from the Lherz orogenic peridotite. *Journal of Petrology*, **31**, 597–628.

BRUIJNE, C. H. & ANDRIESSEN, P. A. 2000. Interplay of intraplate tectonics and surface processes in the Sierra de Guadarrama (central Spain) assessed by apatite fission track analyses. *Physics and Chemistry of the Earth*, **25**, 555–563.

CARIGNAN, J., HILD, P., MEVELLE, G., MOREL, J. & YEGHICHEYAN, D. 2001. Routine analyses of trace elements in geological samples using flow injection and low pressure on-line liquid chromatography coupled to ICP-MS; a study of geochemical reference materials BR, DR-N, UB-N, AN-G and GH. *Geostandards Newsletter*, **25**, 187–198.

DALTON, J. A. & WOOD, B. J. 1993. The composition of primary carbonate melts and their evolution through wallrock reaction in the mantle. *Earth and Planetary Science Letters*, **119**, 511–525.

DEER, W. A., HOWIE, R. A. & ZUSSMAN, J. 1976. *Rock-forming Minerals: Volume 3, Sheet Silicates.* Longman, Harlow.

DOWNES, H. 2001. Formation and modification of the shallow sub-continental lithospheric mantle: a review of geochemical evidence from ultramafic xenolith suites and tectonically emplaced ultramafic massifs of western and central Europe. *Journal of Petrology*, **42**, 233–250.

DOWNES, H. & DUPUY, C. 1987. Textural, isotopic and REE variations in spinel peridotite xenoliths, Massif Central, France. *Earth and Planetary Science Letters*, **82**, 121–135.

DOWNES, H., EMBEY-ISZTIN, A. & THIRLWALL, M. F. 1992. Petrology and geochemistry of spinel peridotite xenoiths from the western Pannonian Basin (Hungary): evidence for an association between enrichment and texture in the upper mantle. *Contributions to Mineralogy and Petrology*, **103**, 277–286.

DOWNES, H., SEGHEDI, I., SZAKACS, A. *ET AL.* 1995. Petrology and geochemistry of late Tertiary/Quaternary mafic alkaline magmatism in Romania. *Lithos*, **35**, 65–81.

DOWNES, H., BALAGANSKAYA, E., BEARD, A., LIFEROVICH, R. & DEMAIFFE, D. 2005. Petrogenetic processes in the ultramafic, alkaline and carbonatitic magmatism in the Kola Alkaline Province: A review. *Lithos*, **85**, 48–75.

DUCEA, M. N. & SALEEBY, J. B. 1998. The age and origin of a thick mafic–ultramafic keel from beneath the Sierra Nevada batholith. *Contributions to Mineralogy and Petrology*, **133**, 169–185.

ESCUDER VIRUETE, J., HERNÁIZ, P. P., VALVERDE, P., RODRÍGUEZ, R. & DUNNING, G. 1998. Variscan syncollisional extension in the Iberian Massif: structural, metamorphic and geochronological evidence from the Somosierra sector of the Sierra de Guadarrama (Central Iberian Zone, Spain). *Tectonophysics*, **290**, 87–109.

ESPERANÇA, S. & HOLLOWAY, J. R. 1987. On the origin of some mica-lamprophyres; experimental evidence from mafic minette. *Contributions to Mineralogy and Petrology*, **95**, 207–216.

FÉMÉNIAS, O., COUSSAERT, N., BINGEN, B., WHITEHOUSE, M., MERCIER, J. C. C. & DEMAIFFE, D.

2003. A Permian underplating event in late- to post-orogenic tectonic setting. Evidence from the mafic–ultramafic layered xenoliths from Beaunit (French Massif Central). *Chemical Geology*, **199**, 293–315.

FERNÁNDEZ-SUÁREZ, J., JEFFRIES, T. E., WHITEHOUSE, M. J., ARENAS, R. & VILLASECA, C. 2006. A U-Pb study of zircons from lower crustal xenoliths of the Spanish Central System: a record of Iberian lithospheric evolution from the Neoproterozoic to the Triassic. *Journal of Geology*, **114**, 471–483.

FOLEY, S. F., JACKSON, S. E., FRYER, B. J., GREENOUGH, J. D. & JENNER, G. A. 1996. Trace element partition coefficients for clinopyroxene and phlogopite in an alkaline lamprophyre from Newfoundland by LAM-ICP-MS. *Geochimica et Cosmochimica Acta*, **60**, 629–638.

FREY, F. A. & PRINZ, M. 1978. Ultramafic inclusions from San Carlos, Arizona; petrologic and geochemical data bearing on their petrogenesis. *Earth and Planetary Science Letters*, **38**, 129–176.

GALINDO, C., HUERTAS, M. J. & CASQUET, C. 1994. Cronología Rb–Sr y K–Ar de diques de la Sierra de Guadarrama (Sistema Central Español). *Geogaceta*, **16**, 23–26.

GARRIDO, C. J. & BODINIER, J. L. 1999. Diversity of mafic rocks in the Ronda Peridotite; evidence for pervasive melt–rock reaction during heating subcontinental lithosphere by upwelling asthenosphere. *Journal of Petrology*, **40**, 729–754.

GREEN, D. H. & WALLACE, M. E. 1988. Mantle metasomatism by ephemeral carbonatite melts. *Nature*, **336**, 459–462.

GRÉGOIRE, M., MOINE, B. N., O'REILLY, S. Y., COTTIN, J. Y. & GIRET, A. 2000. Trace element residence and partitioning in mantle xenoliths metasomatized by highly alkaline, silicate- and carbonate-rich melts (Kerguelen Islands, Indian Ocean). *Journal of Petrology*, **41**, 477–509.

GRÉGOIRE, M., BELL, D. R. & LE ROEX, A. P. 2003. Garnet lherzolites from the Kaapvaal craton (South Africa): trace element evidence for a metasomatic history. *Journal of Petrology*, **44**, 629–657.

HART, S. R. & DUNN, T. 1993. Experimental cpx/melt partitioning of 24 trace elements. *Contributions to Mineralogy and Petrology*, **113**, 1–8.

IONOV, D. A. 1998. Trace element composition of mantle-derived carbonates and coexisting phases in peridotite xenoliths from alkali basalts. *Journal of Petrology*, **39**, 1931–1941.

IONOV, D. A. & HOFMANN, A. W. 1995. Nb–Ta-rich mantle amphiboles and micas: implications for subduction-related metasomatic trace element fractionations. *Earth and Planetary Science Letters*, **131**, 341–356.

IONOV, D. A., GRIFFIN, W. L. & O'REILLY, S. Y. 1997. Volatile-bearing minerals and lithophile trace elements in the upper mantle. *Chemical Geology*, **141**, 153–184.

IONOV, D. A., BODINIER, J. L., MUKASA, S. B. & ZANETTI, A. 2002*a*. Mechanisms and sources of mantle metasomatism: major and trace element compositions of peridotite xenoliths from Spitsbergen in the context of numerical modelling. *Journal of Petrology*, **43**, 2219–2259.

IONOV, D. A., MUKASA, S. B. & BODINIER, J. L. 2002*b*. Sr–Nd–Pb isotopic compositions of peridotite xenoliths from Spitsbergen: numerical modelling indicates Sr–Nd decoupling in the mantle by melt percolation metasomatism. *Journal of Petrology*, **43**, 2261–2278.

IRVING, A. J. & FREY, F. A. 1984. Trace element abundances in megacrysts and their host basalts; constraints on partition coefficients and megacryst genesis. *Geochimica et Cosmochimica Acta*, **48**, 1201–1221.

JOHNSON, K. E., DAVIS, A. M. & BRYNDZIA, L. T. 1996. Contrasting styles of hydrous metasomatism in the upper mantle: an ion microprobe investigation. *Geochimica et Cosmochimica Acta*, **60**, 1367–1385.

KEMPTON, P. D. 1987. Mineralogical and geochemical evidence for differing styles of metasomatism in spinel lherzolite xenoliths: enriched mantle source regions of basalts. *In*: MENZIES, M. & HAWKESWORTH, C. J. (eds) *Mantle Metasomatism*. Academic Press, New York, 45–89.

KEMPTON, P. D., HAWKESWORTH, C. J., LÓPEZ-ESCOBAR, L., PEARSON, D. G. & WARE, A. J., 1999. Spinel ± garnet lherzolite xenoliths from Pali Aike, Part 2: trace element and isotopic evidence on the evolution of lithospheric mantle beneath southern Patagonia. *In*: GURNEY, J., GURNEY, J. L., PASCOE, M. D. & RICHARDSON, S. H. (eds.) *The B. J. Dawson Volume, Proceedings of the 7th International Kimberlite Conference*. Red Roof Design, Cape Town, 415–428.

KLEMME, S., VAN DER LAAN, S. R., FOLEY, S. F. & GÜNTHER, D. 1995. Experimentally determined trace and minor element partitioning between clinopyroxene and carbonatite melt under upper mantle conditions. *Earth and Planetary Science Letters*, **133**, 439–448.

LATOURRETTE, T., HERVIG, R. L. & HOLLOWAY, J. R. 1995. Trace element partitioning between amphibole, phlogopite, and basanite melt. *Earth and Planetary Science Letters*, **135**, 13–30.

LITASOV, K. D., FOLEY, S. F. & LITASOV, Y. D. 2000. Magmatic modification and metasomatism of the subcontinental mantle beneath the Vitim volcanic field (East Siberia): evidence from trace element data on pyroxenite and peridotite xenoliths from Miocene picrobasalt. *Lithos*, **54**, 83–114.

MATTIELLI, N., WEIS, D., SCOATES, J. S. *ET AL.* 1999. Evolution of heterogeneous lithospheric mantle in a plume environment beneath the Kerguelen Archipelago. *Journal of Petrology*, **40**, 1721–1744.

MCDONOUGH, W. F. & SUN, S. S. 1995. The composition of the Earth. *Chemical Geology*, **120**, 223–253.

MERCIER, J. C. C. 1980. Single-pyroxene thermobarometry. *Tectonophysics*, **70**, 1–37.

MINARIK, W. G. 1998. Complications to carbonate melt mobility due to the presence of an immiscible silicate melt. *Journal of Petrology*, **39**, 1965–1973.

NAVON, O. & STOLPER, E. 1987. Geochemical consequences of melt percolation; the upper mantle as a chromatographic column. *Journal of Geology*, **95**, 285–307.

NIMIS, P. & ULMER, P. 1998. Clinopyroxene geobarometry of magmatic rocks Part 1: An expanded structural geobarometer for anhydrous and hydrous, basic and ultrabasic systems. *Contributions to Mineralogy and Petrology*, **133**, 122–135.

O'REILLY, S. Y., GRIFFIN, W. L. & RYAN, C. G. 1991. Residence of trace elements in metasomatized spinel lherzolite xenoliths; a proton–microprobe study. *Contributions to Mineralogy and Petrology*, **109**, 98–113.

OREJANA, D., VILLASECA, C. & PATERSON, B. A. 2006. Geochemistry of pyroxenitic and hornblenditic xenoliths in alkaline lamprophyres from the Spanish Central System. *Lithos*, **86**, 167–196.

OTTEN, M. T. 1984. The origin of brown hornblende in the Artfjaellet gabbro and dolerites. *Contributions to Mineralogy and Petrology*, **86**, 189–199.

PAWLEY, A. R. 2003. Chlorite stability in mantle peridotite: the reaction clinochlore + enstatite = forsterite + pyrope + H_2O. *Contributions to Mineralogy and Petrology*, **144**, 449–456.

PAWLEY, A. R. & WOOD, B. J. 1995. The high pressure stability of talc and 10 Å phase: Potential storage sites for H_2O in subduction zones. *American Mineralogist*, **80**, 998–1003.

PERINI, G., CEBRIÁ, J. M., LÓPEZ-RUIZ, J. M. & DOBLAS, M. 2004. Permo-Carboniferous magmatism in the variscan belt of Spain and France: implications on mantle sources. *In*: WILSON, M., NEUMANN, E. R., DAVIES, G. R., TIMMERMAN, M. J., HEEREMANS, M. & LARSEN, B. (eds) *Permo-Carboniferous Magmatism and Rifting in Europe*. Geological Society, London, Special Publications, **223**, 415–438.

REYES, J., VILLASECA, C., BARBERO, L., QUEJIDO, A. J. & SANTOS, J. F. 1997. Descripción de un método de separación de Rb, Sr, Sm y Nd en rocas silicatadas para estudios isotópicos. *In: Actas del I Congreso Ibérico de Geoquímica*. CEDEX, Soria, 46–55.

ROCK, N. M. S. 1991. *Lamprophyres*. Blackie, Glasgow.

ROSENBAUM, M. J., WILSON, M. & DOWNES, H. 1997. Enrichment of the Pannonian Carpathian mantle: Pb–Sr–Nd isotope and trace element constraints. *Journal of Geophysical Research*, **102**, 14947–14961.

SCARROW, J., BEA, F., MONTERO, P., MOLINA, J. F. & VAUGHAN, A. P. M. 2006. A precise late Permian $^{40}Ar/^{39}Ar$ age for Central Iberian camptonitic lamprophyres. *Geologica Acta*, **4**, 451–459.

SHAW, C. S. J. 2004. The temporal evolution of three magmatic systems in the West Eifel volcanic field, Germany. *Journal of Volcanology and Geothermal Research*, **131**, 213–240.

SKULSKI, T., MINARIK, W. & WATSON, E. B. 1994. High-pressure experimental trace-element partitioning between clinopyroxene and basaltic melts. *Chemical Geology*, **117**, 127–147.

SUN, S. S. & MCDONOUGH, W. F. 1989. Chemical and isotopic systematics of oceanic basalts; implications for mantle composition and processes. *In*: SAUNDERS, A. D. & NORRY, M. J. (eds) *Magmatism in Ocean Basins*. Geological Society, Special Publications, **42**, 313–345.

VASELLI, O., DOWNES, H., THIRLWALL, M. F. *ET AL.* 1995. Ultramafic xenoliths from Plio-Pleistocene alkali basalts from the Eastern Transylvanian Basin: depleted mantle enriched by vein metasomatism. *Journal of Petrology*, **38**, 23–54.

VERNIÈRES, J., GODARD, M. & BODINIER, J. L. 1997. A plate model for the simulation of trace element fractionation during partial melting and magmas transport in the Earth's upper mantle. *Journal of Geophysical Research*, **102**, 24771–24784.

VILLASECA, C., DOWNES, H., PIN, C. & BARBERO, L. 1999. Nature and composition of the lower continental crust in Central Spain and the granulite-granite linkage: inferences from granulitic xenoliths. *Journal of Petrology*, **40**, 1465–1496.

VILLASECA, C., OREJANA, D., PIN, C., LÓPEZ GARCÍA, J. A. & ANDONAEGUI, P. 2004. Le magmatisme basique hercynien et post-hercynien du Système Central Espagnol: essai de caractèrisation des sources manteliques. *Comptes Rendus de Géosciences*, **336**, 877–888.

WILSHIRE, H. G., 1987. A model of mantle metasomatism. *In*: MORRIS, E. M. & PASTERIS, J. D. (eds) *Mantle Metasomatism and Alkaline Magmatism*. Geological Society of America, special papers, **215**, 47–60.

WILSON, M. 1989. *Igneous Petrogenesis: a Global Tectonic Approach*. Unwin Hyman, Boston, MA.

WITT-EICKSCHEN, G., SECK, H. A., MEZGER, K., EGGINS, S. M. & ALTHERR, R. 2003. Lithospheric mantle evolution beneath the Eifel (Germany): constraints from Sr–Nd–Pb isotopes and trace element abundances in spinel peridotite and pyroxenite xenoliths. *Journal of Petrology*, **44**, 1077–1095.

WOOLLEY, A. R. & KEMPE, D. R. C. 1989. Carbonatites: nomenclature, average chemical compositions, and element distribution. *In*: BELL, K. (ed.) *Carbonatites: Genesis and Evolution*. Unwin Hyman, London, 1–14.

XU, X., O'REILLY, S. Y., GRIFFIN, W. L. & ZHOU, X. 2003. Enrichment of upper mantle peridotite: petrological, trace element and isotopic evidece in xenoliths from SE China. *Chemical Geology*, **198**, 163–188.

XU, Y. G. 2002. Evidence for crustal components in the mantle and constraints on crustal recycling mechanisms: pyroxenite xenoliths from Hannuoba, North China. *Chemical Geology*, **182**, 301–322.

XU, Y. G. & BODINIER, J. L. 2004. Contrasting enrichments in high- and low-temperature mantle xenoliths from Nushan, eastern China: results of a single metasomatic event during lithospheric accretion. *Journal of Petrology*, **45**, 321–341.

YAXLEY, G. M., GREEN, D. H. & KAMENETSKY, V. 1998. Carbonatite metasomatism in the southeastern Australia lithosphere. *Journal of Petrology*, **39**, 1917–1930.

ZANETTI, A., VANNUCCI, R., BOTTAZZI, P., OBERTI, R. & OTTOLINI, L. 1996. Infiltration metasomatism at Lherz as monitored by systematic ion-microprobe investigations close to a hornblendite vein. *Chemical Geology*, **134**, 113–133.